Environmental Earth Sciences (2023) 82:277
https://doi.org/10.1007/s12665-023-10966-4

ORIGINAL ARTICLE

Analysis of the pore network structure of microbial solidification of construction residue soil based on CT scanning

Zhang Minxia[1] · Feng Congrui[1] · Niu Shuangjian[2] · Xu Ping[1] · Chen Chen[1]

Received: 6 September 2022 / Accepted: 7 May 2023 / Published online: 22 May 2023

Abstract

The pore structure of microbially solidified construction residue soil is an important factor affecting its ability to resist wind erosion and dust. It is challenging to explain the mechanism of microbially induced calcium carbonate precipitation and to more accurately simulate the infiltration process of bacterial liquid given that current studies on pore structure and distribution in this field are restricted to two-dimensional surface observation and macroscopic experimental parameter determination. In this paper, the high-precision image of microbially solidified construction residue soil is obtained by CT scanning, and the three-dimensional network pore structure model of microbially solidified construction residue soil is reconstructed using advanced visualization software (Avizo) and digital image processing technology. Four representative units are extracted from the model in turn, and the maximum ball algorithm is used to statistically analyze the parameters such as pores and throats of the representative units. Results show that the soil's pore and throat radii are, respectively, distributed around 80 and 60 μm and the fitting indexes are 0.90 and 0.93, respectively. The coordination number is mainly distributed in the range of 4–11, and the fitting index is 0.94. The throat length is distributed in the range of 50–950 μm, and the fitting index is 0.83. According to frequency distributions of pore volume and pore-throat equivalent radius ratio, the pores in the soil are mostly small and micro pores, the pore network is well developed, and the structure is relatively stable. Construction residue soil's resistance to wind erosion and dust-raising can be significantly improved by microbial solidification. This method can also be useful for nondestructive quantitative characterization of soil meso-pore network structure.

Keywords Microbial solidification · Construction residue soil · Pore network · CT scanning · Maximum ball algorithm · Parametric analysis

Introduction

Biogeotechnology has many advantages, such as low carbon, environmental protection, as well as low investment and maintenance costs. It is mainly used to deal with environmental control, soil reinforcement, slope protection, and building crack repair.

Soil is the most complex nonlinear system in the world. The reason for its complexity is that the internal pore network structure changes all the time. In the field of soil improvement in geotechnical engineering, pouring cement or chemical materials into the soil is a common technique for soil reinforcement. Nevertheless, this technique often poses a serious threat to the environment (Dimitrios and Lyesse 2019; DeJong et al. 2010), so scientists are striving to develop an eco-friendly soil reinforcement technology. Microbially induced carbonate precipitation (MICP) is a new type of soil reinforcement technology that is green, easy to operate and efficient (Whiffin 2004; Mitchell and Santamarina 2005). The mechanism of MICP is that microorganisms produce mineral crystals through a series of biochemical reactions with the surrounding environment using their own metabolism and respiration, and then use their filling and cementation to fill soil pores (DeJong et al. 2006), changing the pore network structure of the soil, improving soil stability and giving loose soil specific mechanical properties (Ivanov and Chu 2008; Cheng et al. 2013; Tang et al. 2020; Whiffin et al. 2007; Michael et al. 2016).

✉ Feng Congrui
fx2022513@163.com

[1] School of Civil Engineering, Henan Polytechnic University, Jiaozuo 454003, China

[2] Shenzhen Municipal Engineering Corporation, Shenzhen 518131, Guangdong, China

The impermeability of rock and soil mass (Cuthbert et al. 2013; Phillips et al. 2016), soil improvement (Liu et al. 2016; Van Paassen et al. 2010), anti-liquefaction (Montoya et al. 2013; DeJong et al. 2013), freeze–thaw resistance (Cheng et al. 2013; Sharma et al. 2021), dust suppression and sand fixation (Naeimi and Chu 2017; Meyer et al. 2011), and treatment of polluted soil (Xu et al. 2013; Fujita et al. 2010), are the main areas of research and application for microbial solidification technology in the field of geotechnical engineering. Currently, the most efficient MICP is achieved through microbiologically or enzymatically catalyzed urea hydrolysis, whereby soluble calcium source is converted into insoluble calcium carbonate crystals that bind individual soil grains together, forming a thin layer of calcium carbonate crust to withstand wind erosion and dust, which has become a hot topic in the engineering world. Meng et al. (2021a; b) carried out a field test to study the ability of microbially solidified desert soil to resist wind erosion; results show that microbial solidification can form crusts on the soil surface, thereby improving the bearing capacity and wind erosion resistance of desert soil. Zhang et al. (2021) performed wind tunnel tests on four groups of microbially consolidated sands with different particle sizes, and analyzed the surface strength, microstructure, and soluble salt content of the samples before and after the test; they concluded that microbially consolidated bare soil is an efficient and environmentally friendly anti-wind erosion and dust technology. Zhan et al. (2016) determined through laboratory tests and engineering applications that microbial solidification of soil technology can effectively improve soil resistance to wind and hydraulic erosion and has good ecological compatibility. The essence of microbially solidified soil is that in the pore network inside the soil, either the mineral crystals produced by microbial solidification are adsorbed on the surface of soil particles to increase the particle size, or the adjacent soil particles are bonded together by "biological bridging", in order to improve the stability of soil pore structure and achieve the purpose of improvement. However, the majority of current research on microbially solidified soil focuses on its macroscopic mechanical properties, and there are only a few mesoscopic studies on the pore network structure within the soil (Terzis and Laloui 2018, 2019), which does not support the potential application of microbial solidification and soil improvement technology.

The main purpose of this article is to study how to use the MICP process for changing soil pore structure, i.e., to improve the anti-wind erosion and dust-raising ability of construction residue soil. The microbially solidified construction residue soil is scanned by CT, and the original image obtained from the scan is de-noised, enhanced, and thresholded by the advanced visualization software Avizo. The pore network model of the soil is three-dimensionally reconstructed. At the same time, the overall pore network is characterized using a set of representative units of a certain size, and the frequency distribution histogram and curve of the extracted parameters are analyzed using the pore size, throat length, pore coordination number, pore volume, pore-throat ratio, and other parameters of the characterizing unit body. It can be used as a reference for future studies on the characterization of microbially solidified soil structure and the characteristics of wind erosion and dust resistance.

Materials and methods

Test soil

The soil sample used in this experiment is the construction residue soil in the mountain area of Jiaozuo, Henan Province. The construction residue soil usually refers to the abandoned soil containing various building materials and other wastes produced in building construction or demolition processes. This type of soil has no cohesive force holding the particles, and it easily produces dust when it is piled up on a construction site, which pollutes the environment. The soil sample is taken to the laboratory for natural air drying, and crushed through a 2 mm sieve, to maintain its basic physical properties. Although the soil cannot be completely dried under natural conditions, the water content after air drying is defined as the minimum water content under natural conditions. The grain size distribution curve of the soil after screening is determined by laser particle size analyzer (Fig. 1), as shown in Fig. 2. The uneven coefficient $Cu = 7.27 > 5$ and the curvature coefficient $Cc = 1.22 = 1–3$ can be obtained from the data in Fig. 2, namely, the soil with good gradation. The basic physical soil indexes are determined according to the soil test standard GB/T50123-2019, and the results are shown in Table 1.

Fig. 1 Laser particle analyzer

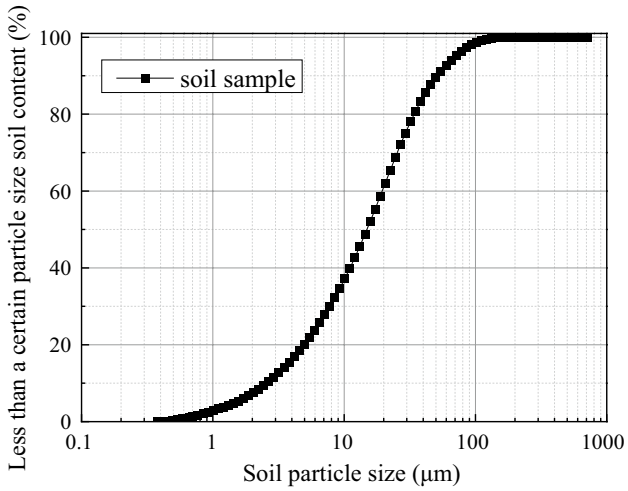

Fig. 2 The gradation curve of soil particle size

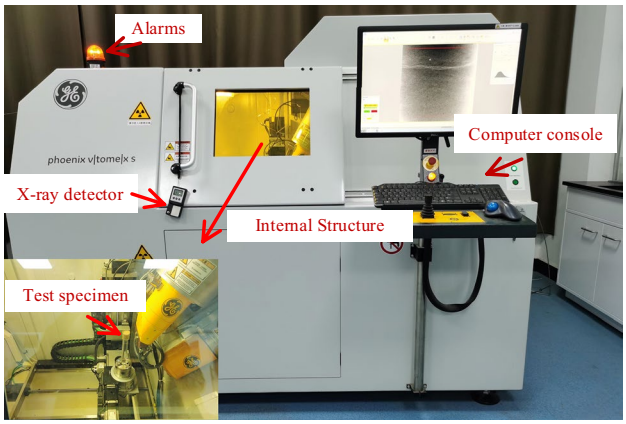

Fig. 3 Industrial microscopic CT scanning system

CT scanning and sample preparation

The mercury injection capillary pressure and nitrogen adsorption methods are distinct from CT scanning. These two techniques can extract the pore size distribution and pore volume of rock and soil, but they are unable to accurately characterize the pore network structure of soil or extract the closed pores, and they may also damage the sample (Wu et al. 2019) to some extent. CT scanning technology has the characteristics of being non-destructive and real-time, which allows to observe the internal structure of the sample in real time without altering its state (Li et al. 2016), such as pore size, medium size, pore network distribution and compactness change. It also allows the direct observation of closed pores and their characteristics. In this experiment, Phoenix v| tome |x s, an industrial microscopic CT scanning system is used for nondestructive scanning of the three-dimensional structure of the soil sample. As shown in Fig. 3, the system was produced by General Electric Co., Ltd. and it is a multi-functional high-resolution system for two-dimensional X-ray detection, three-dimensional computer tomography, and three-dimensional measurement. The chosen CT scanning parameters for soil samples after system debugging are: voltage 150 kV, current 130 μA, exposure time 1000 m/s, sensitivity 2, and image resolution 11.54 μm. A total of 1500 jpg images (1936 × 1936 pixels, 8-bit gray value) scanned in the default order are collected.

The specimen used for scanning is a construction residue soil prepared in a 10 ml beaker as a mold. The specimen preparation process is carried out using the controlled dry density method to fill the mold with the test soil, and the upper surface of the soil is spread flat. Next, the microbial curing test is carried out using the most common and efficient reaction process, namely the urea hydrolysis reaction process (Phillips et al. 2013). The strain used is *Bacillus Sporosarcina pasteurii* (China General Microorganism Collection and Management Center No. CGMCC1.3687), and the cementing solution is a mixture of urea and calcium chloride in equal proportion. The urease produced by *Bacillus Sporosarcina pasteurii* metabolism is used to hydrolyze urea in a series of biochemical reactions, with *Bacillus Sporosarcina* as the nucleation site. The reaction process then precipitates calcium carbonate crystals with cementation and fills the final nucleation site of *Bacillus* sp. The spraying method (Cheng and Cord-Ruwisch 2014) is used in this experiment to carry out the microbial curing of the soil surface. Table 2 shows the amounts and concentrations of the bacterial solution and the cementing solution. Specimens were sprayed with bacterial solution first, followed by colloidal solution at intervals of ten minutes, and then kept at room temperature for seven days after spraying. Afterwards, a CT scan of the mold's central cylinder (20 mm height × 20 mm diameter at the bottom) was performed, as shown in Fig. 4.

Table 1 Basic physical indexes of soil samples

Soil sample	Natural density (kN m^{-3})	Maximum dry unit density/(g cm^{-3})	Minimum dry unit density/(g cm^{-3})	Liquid limit (%)	Plastic limit (%)	D_{50} (μm)	D_{90} (μm)
Construction residue soil	1.67	1.51	1.00	24.6	16.7	12.36	36.82

Table 2 Parameter design for microbially solidified construction residues soil

Dry density/ (g cm^{-3})	Bacterium dosage/ (L m^{-2})	Cement dosage/ (L m^{-2})	Bacterial concentration/ (OD_{600})	Cement concentration/ (mol L^{-1})	Curing time/ (d)
1.357	0.5	1.0	4.0	0.5	7

Fig. 4 Microbial consolidation of soil samples for CT scan

Max ball algorithm

The maximum ball algorithm is a method for characterizing the pore network structure of porous media using a ball-and-stick model, which typically uses data from microscopic CT scan imaging. It employs a three-dimensional binary matrix transport algorithm to model and analyze the images in order to describe the physical and mechanical characteristics of porous media. The algorithm was first proposed by Silin and Patzek (2006) based on the pore network model proposed by Fatt (1956), which defines the concept of pore body and pore throat. The pores in the soil are identified as inner tangent spheres, and the connected inner tangent spheres represent connected pores. The modeling automatically identifies the largest and smaller spheres in the inner tangent spheres. The largest sphere is identified as the ball and the connected smaller spheres are modeled as the stick in the ball-and-stick model. The connected spheres form the ball-and-stick model to characterize the pore network structure of the medium. However, determining the boundary between the pores and the throat channel is not an easy task, because there is no clear definition of the complete soil pore network that Silin and Patzek (2006) failed to extract. Al-Kharusi and Blunt (2007) extended Silin's ball-and-stick model in 2007 to include the concept of master spheres, slave spheres, or star cluster spheres to analyze the pore network structure of the medium in a more refined way, but the practicality of Al-Kharusi algorithm is weak due to the pore number limitation. Dong and Blunt (2009) abandoned the previous classification of spheres and distinguished the pore network structure into pores and throats only and improved the original maximum ball algorithm. They extracted the simplified pore-throat network from the pore space image by parameterizing the geometric structure and connectivity, predicted the sandstone pore space network model's relative permeability based on the extracted parameters, and compared with the experimental results to verify the reliability of the maximum ball algorithm.

Avizo is an advanced 3D visualization tool for materials science, with features like raw image preprocessing, threshold segmentation, 3D volume rendering, pore network reconstruction, and geometric surface meshing. It can also analyze the relevant parameters of the matrix and pore body in the 3D-reconstructed model and save the data in other relevant formats for joint numerical simulation using COMSOL and ANSYS (Bird et al. 2014; Fan et al. 2020). In this paper, Avizo is used to apply a series of processing functions on raw images obtained from CT scans. The Pore Network Model View module of the software is used to visualize the pore network model of the 3D-reconstructed model with a ball-stick visualization, and to characterize and analyze the soil pore network based on the data obtained from the maximum ball algorithm (Xie et al. 2020) to assess its structural stability.

The formulas of the maximum ball algorithm based on the 3D visualization software Avizo (Li et al. 2019) are given in (1)–(6):

Pore (throat) length (L):

$$L = \sum_{i=1}^{n} l_i, \tag{1}$$

where l_i is the discrete pore length (μm) divided by a number of points equal to the Euclidean distance between two points.

Pore (throat) volume (V_p):

$$V_p = N \times V_0, \tag{2}$$

where V_0 is the volume of the smallest voxel unit (μm^3), and N is the number of voxel units contained in the 3D pores.

Pore equivalent radius (R_p):

$$R_p = \frac{\sqrt[3]{\frac{6V_p}{\pi}}}{2}, \tag{3}$$

Throat equivalent radius (R_t):

$$R_t = \frac{\sqrt{\frac{4V_p}{\pi L}}}{2}, \tag{4}$$

where V_p is the pore volume (μm^3), and L is the pore length (μm).

Coordination number (C):

$$C = \frac{2 \times N_B - N_E}{N_J}, \tag{5}$$

where N_B is the number of branch pores connected by a node, N_E is the number of endpoint pores, and N_J is the number of nodes.

Pore throat equivalent radius ratio (P):

$$P = \frac{R_{pi}}{R_{ti}}, \tag{6}$$

where R_{pi} is the equivalent radius of the ith pore sphere, R_{ti} is the equivalent radius of the throat connected to the ith pore sphere.

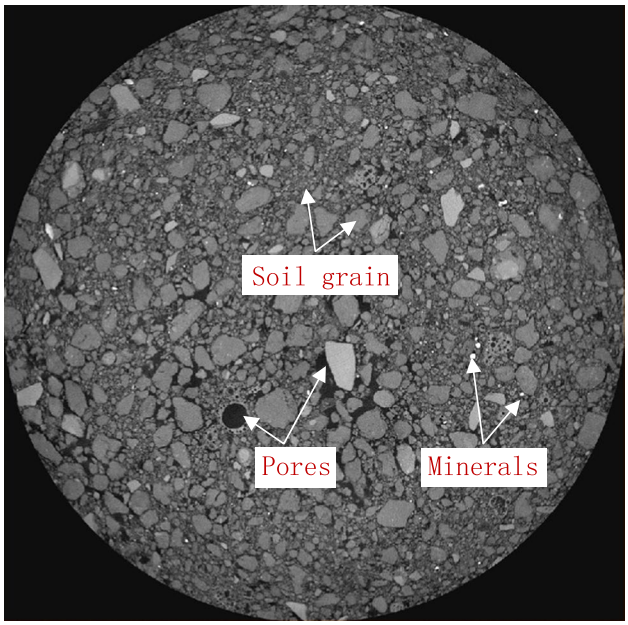

Fig. 5 Two-dimensional tomographic image of soil [threshold range: pores (54–92), soil grain (92–175), minerals (175–250)]

Reconstruction of the 3D pore network model

Image processing

Figure 5 shows the two-dimensional construction residue tomographic image obtained from industrial micro-CT scan. There are three colors in the image: white, black, and gray. The white area indicates the high-density area, which represents the minerals in the soil sample. The black part indicates the low-density area, thus showing the pores in the soil body, and the darker black parts indicate the more developed pores inside the specimen. The remaining gray parts represent the soil agglomerates and soil particles. The purpose of this paper is to explore the pore network model of the soil body, so when thresholding the CT images, minerals, soil aggregates, and soil particles are segmented as solid-phase factors of the soil body to facilitate the modeling and the analysis of the soil pore network structure parameters. The two-dimensional tomographic sections can only show the distribution information of soil matrix and pores in the specimen cross-section, which cannot visually characterize the three-dimensional structure of the soil body (Ivanov et al. 2019). Therefore, the Avizo 3D reconstruction technique is required to convert a series of 2D tomographic images obtained from the scan into a three-dimensional structure, in order to observe the fine-scale structure of the soil sample pore network more intuitively.

In the CT scanning of soil samples, some small spots often appear on the original CT images due to soil disturbance, and unstable operating voltage and current of the scanning equipment and detector noise, which affects the modeling of the soil to some extent in the later 3D reconstruction. In order to minimize the impact of such factors on image quality, a noise reduction filter is applied, edges are enhanced, and other pre-processing techniques are performed on the original CT images to improve the analysis of the structural information of the pore network of the construction residue soil later on. Common filtering methods are Gaussian filtering, mean filtering and median filtering. In this paper, the median filter of the filter sandbox module of Avizo is first applied to smooth the original images. Median filtering is more efficient than the other two filtering methods and results in a smoother output. It reduces the noise at image edges while maintaining the effective information in the image (Fig. 6).

3D reconstruction and extraction of characterization units

The three-dimensional model of the CT-scanned images of microbially solidified soil is reconstructed using the visual image analysis software Avizo. The preprocessed two-dimensional CT fault image is first segmented by binarization. Based on gray level differences in the CT image, the interactive thresholding module in Avizo is used with the appropriate threshold to segment the CT image. Segmentation is a key step in the subsequent modeling analysis. In this paper, the soil is mainly divided into two states, pores and solid phases. There are many small pores in the soil due to

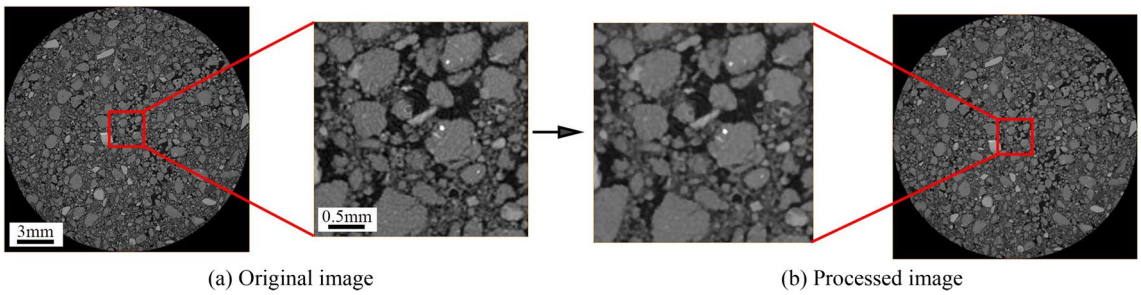

Fig. 6 Pre-processing effect of the original image

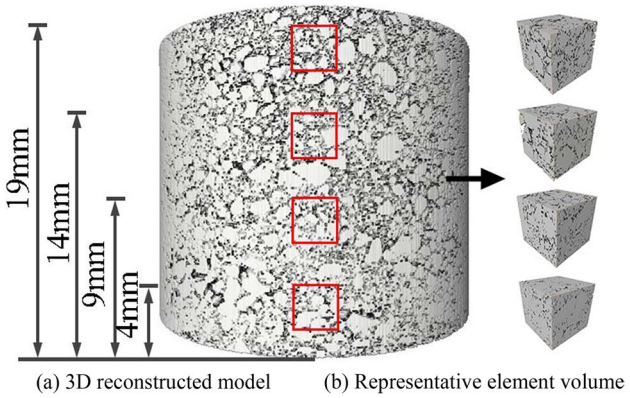

Fig. 7 Extraction of representative element volume

its looseness. For these small pores, the interactive Top-Hat module can be used to better identify the fine structure in the segmented image. The volume rendering module is then used to reconstruct the 3D image of the soil, which is shown in Fig. 7a. As seen in the diagram, the soil particle content has an absolute advantage, and the interactive distribution of pores forms a connected network structure. Due to the limitation of computer memory and CPU processing capacity, a representative element volume (REV) of $3 \times 3 \times 3$ mm is taken every 2 mm in the three-dimensional reconstruction model of soil to characterize the pore network parameters of this layer in the residual soil (Koestel et al. 2020). Four REVs are taken from top to bottom, as shown in Fig. 7b. The three-dimensional pore network structure of the soil representative element REV is visualized, and the qualitative extraction and analysis of relevant parameters are carried out to clearly understand the meso-structure characteristics of the pore network in the microbially solidified soil.

Parametric analysis of the extracted REV pore network model (Brian and Robert 1998) is performed based on the maximum ball algorithm. The Volume Edit module in Avizo is first used to extract the corresponding position and characterize the three-dimensional structure of the unitary REV. The Axis Connectivity module is then used to link the pores in the REV and remove the isolated pores. The Separate Objects module is used next, in order to adjust the relevant parameters to segment the pores in the REV. The individual pores are characterized as shown in Fig. 8c, and the pore network model of REV is modeled using the Generate Pore Network Model function as shown in Fig. 8d. The maximum ball algorithm is analyzed using the Pore Network Model View module, and the relevant parameters of the pore network structure model of the soil REV are finally exported. In the reconstructed REV pore network ball-and-stick model, the ball represents the pores and the cylinder represents the throat channel connected between the pores. In this paper, the REV pore network model is analyzed by the maximum ball algorithm to obtain the structural parameters, such as

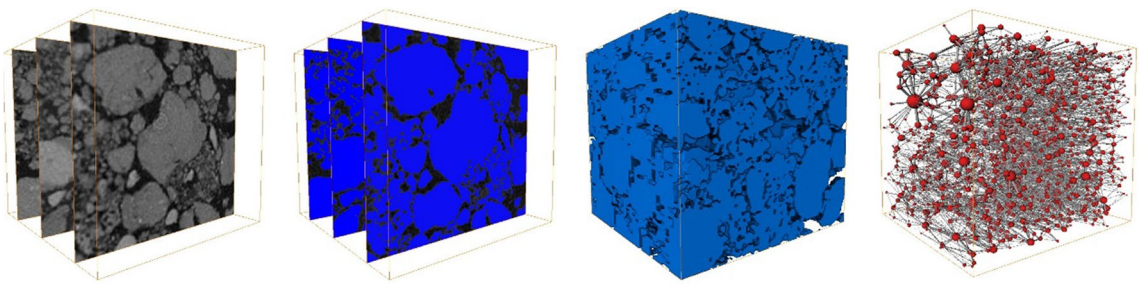

Fig. 8 REV pore structure reconstruction

pores and throat channels of the REV, distribution of the volume of pores, equivalent radius of pores, coordination number, equivalent radius of throat channels, and length of throat channels. Pore-throat radius ratio (Meng et al. 2021a, b) in the soil REV is evaluated by analysis to describe the overall pore network distribution characteristics and structural stability of the soil sample.

Parameter results and analysis

Comprehensive analysis of the four REV pore network models extracted from the 3D reconstructed model and the statistics of the relevant pore parameters is carried out, and the frequency distribution of each parameter is plotted. Figures 9 and 10 show the frequency and distribution curves of pore equivalent radius and throat equivalent radius, respectively. It can be observed that the pore equivalent radius distribution is within 250 μm, with a peak frequency distribution of about 9% near 80 μm. The number of pores with equivalent radius in the range of 70–100 μm accounts for most of the pores, and there is only a very small number of pores with equivalent radius over 150 μm and below 40 μm. The distribution of the equivalent radius of the throat channels is also within 250 μm, and the frequency distribution peak occurs around 60 μm, which is about 10%. The number of throat channels with the equivalent radius in the range of 40–70 μm accounts for the majority, and the throat channels with the equivalent radius over 120 μm represent a minority. This indicates that the pore spaces in the range of 70–100 μm and the throat channels in the range of 40–70 μm are the main components in the pore network structure of this soil sample. The equivalent radius of the pore and the equivalent radius of the throat are fitted with Gaussians. The average equivalent radius of the pore is 110 μm, and the fitted index

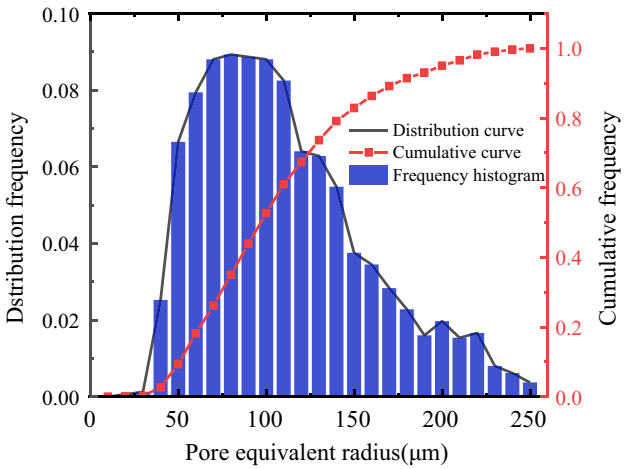

Fig. 9 REV pore radius distribution frequency figure

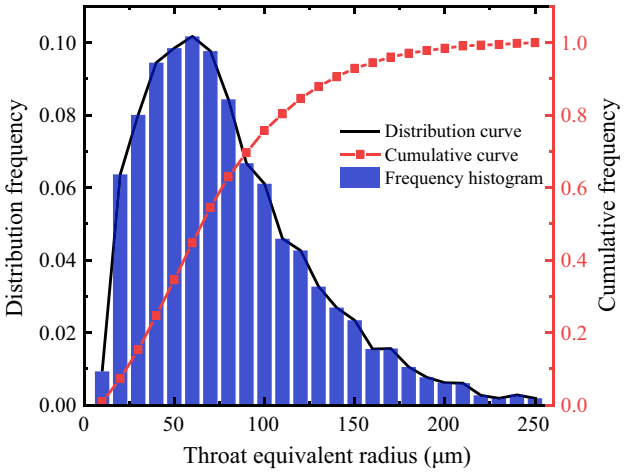

Fig. 10 REV throat radius distribution frequency figure

after the adjustment of the pore radius is 0.90. The average equivalent radius of the throat is 79 μm, and the fitted index after the adjustment of the throat radius is 0.93. It can be seen that the frequency distribution curves of the pore radius and the throat radius approximately obey the normal distribution. The frequency distributions of pore and throat dimensions of the four characterization units indicate that the overall structure of the soil body is relatively stable.

In the three-dimensional reconstruction of soil body, the pores are connected to one another by the throat. The number of pore throats connected to a pore is called the coordination number of the pore, which can directly indicate the good or bad connectivity of the pore network. The connectivity between the pores improves with increasing coordination number, and the permeability of the three-dimensional pore structure model to the medium also improves with connectivity. Figure 11 shows the frequency diagram of the average coordination number distribution of the four taken REVs. It can be observed in the figure that the coordination number of the soil sample is mostly distributed in the interval from 0 to 25, where the peak frequency distribution occurs near the coordination number of 6, which is about 12%. Since the sample is a soil structure, there are almost no closed pores when the coordination number is 0, meaning that the pores are closed and not connected to other pores. The percentage of the four REV pore parameters is 0.1% in this case. The average coordination number of all pores in the soil is 9.03. The Gaussian fitting of the coordination number frequency distribution curve shows that the fitting index of the coordination number is 0.94, which indicates that the frequency distribution curve roughly follows the normal distribution, which suggests that the coordination number distribution is more concentrated and the pore network of the soil is better connected.

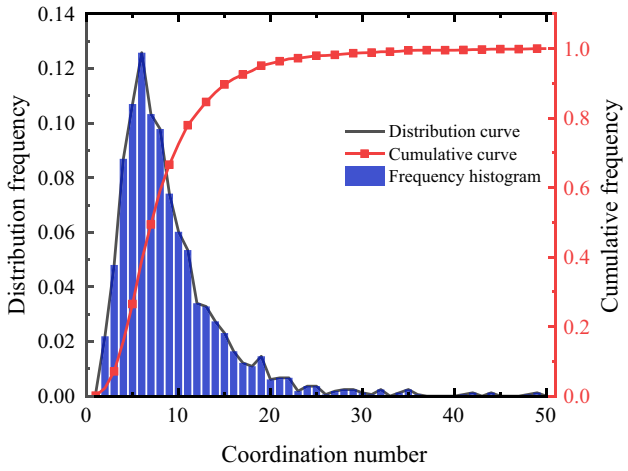

Fig. 11 REV coordination number distribution frequency figure

Figure 12 shows the frequency distribution diagram of four REV throat lengths. It can be noticed that most of the throat lengths are distributed in the range of 50–950 μm, and the frequency distribution peak appears near the throat length of 180 μm, accounting for about 9%. Gaussian curve fitting is used to fit the distribution frequency of the throat length. The fitting index of the throat length is 0.83, and the average equivalent length of the throat is 380 μm, which is quite different from the peak value of the throat. However, as can be seen from the figure, the frequency distribution of the throat length is relatively concentrated. When the throat length exceeds the 180 μm peak, the distribution frequency of throat length shows a gradual decreasing trend, indicating that the throat length is roughly subject to normal distribution. This corresponds to the normal distribution frequency of pore and throat equivalent radius, indicating that the pore network structure of soil is relatively stable.

Figure 13 shows the frequency diagram of the pore volume distribution of the four REVs. It can be observed that the distribution of the pore volume of the soil sample is relatively uneven, due to the fragmentation and dispersion of the soil, and most of the pore volume is in $0–1.0\times10^7$ μm^3, accounting for 83%, while only 15% of the pore volume exceeds 2.0×10^7 μm^3. The frequency distribution curve of the pore volume is fitted with a Gaussian, and the correlation coefficient obtained from the fitting is 0.52. Therefore, the distribution curve does not follow a normal distribution. The reason is that due to the special nature of the soil, most of the pore network is made up of small pores and micro-pores. However, this also demonstrates that the skeletal part of the soil is completely dominant, and the structure is stable.

In the soil REV pore network structure, the ratio of the equivalent radius of the pore and the equivalent radius of its connected throat is defined as the pore-throat radius ratio. By reflecting the size difference between the pore and its connected throat, this ratio can, to a certain extent, reflect the uniformity of the development of the pore network structure. The smaller the radius ratio of pore throat, the smaller the size difference of pore throat, the more uniformly the pore network develops, and the structure is relatively stable. In contrast, the larger the pore throat radius ratio, the larger the size difference of pore throat, the poorer the pore network develops, the larger the size difference of pore and throat, and the structure is very unstable. Figure 14 shows the frequency diagram of REV pore-throat equivalent radius ratio distribution. As can be seen from the diagram, the pore-throat radius ratio is mainly distributed in the range of 0.5–2.0, accounting for 64%, while the pore-throat ratio over 3.0 accounts for very little. Through the analysis of the REV pore-throat radius ratio, it shows that the pore network of the samples is relatively uniformly developed, and the structure is more stable. Due to the properties of the soil, there are

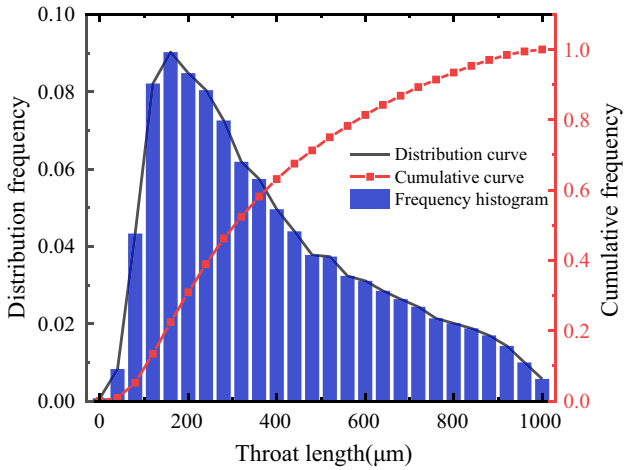

Fig. 12 REV throat length distribution frequency figure

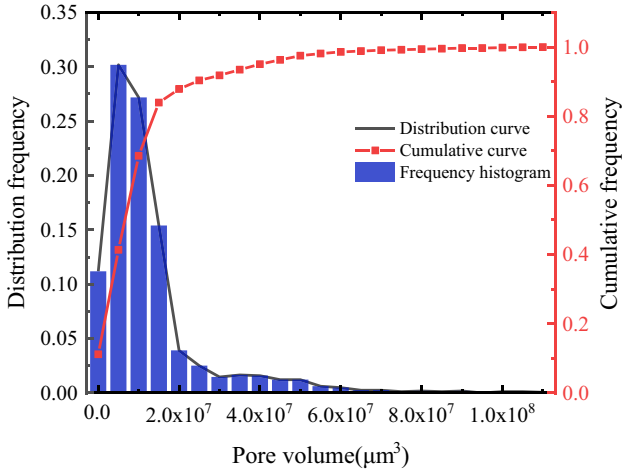

Fig. 13 REV pore volume distribution frequency figure

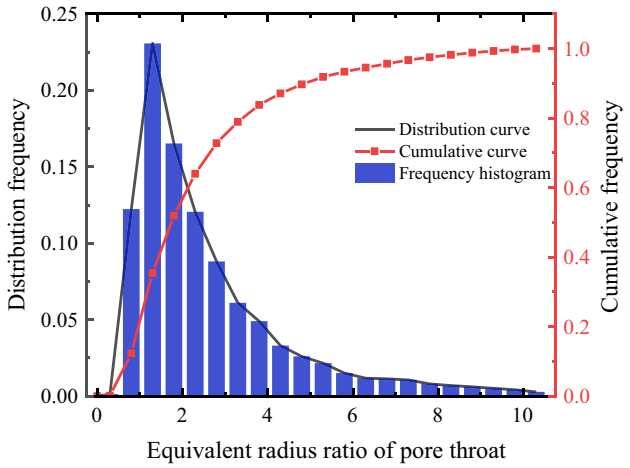

Fig. 14 REV pore throat radius ratio distribution frequency figure

some areas with a large pore throat radius, but the proportion is generally quite small, so the overall soil structure is relatively stable.

Conclusion

(1) A high-precision image was obtained by CT scanning of microbially solidified construction residue soil. The visualization software Avizo and digital image processing technology were used for denoising, enhancement, threshold segmentation, and three-dimensional volume rendering of CT scanning images. The three-dimensional pore network model of microbially solidified construction residue soil was reconstructed. Four REVs were extracted from the model, and the maximum ball algorithm was used to analyze the pore network structure of the REV.

(2) The analysis of the pore parameters of the soil REV pore network model showed that the pore radius, throat radius, pore coordination number, and throat length all roughly follow a normal distribution, and the frequency distributions of pore volume and pore-throat equivalent radius ratio are also more concentrated, indicating that the pore network of microbially cured construction residue soil is more evenly developed and features a more stable structure.

(3) The pore and throat radii are, respectively, distributed in the range of 80 and 60 μm, and their fitting indexes are 0.90 and 0.93, respectively. The coordination number is mainly distributed in the range of 4–11, and the fit index is 0.94. The throat length is distributed in the range of 50–950 μm, and the fit index is 0.83. The pore volume is mostly less than 1.0×10^7 μm^3, accounting for 83%, the pore-throat radius ratio is mainly distributed in the range of 0.5–2.0 accounting for 64%, and the ratio of more than 3.0 is very small.

According to this study's analysis of the meso-structure of the soil pore network, microbial curing directly increases the soil's wind erosion resistance while also improving the pore network of construction residue. This suggests that microbial curing technology has a lot of potential in the field of geotechnical engineering soil reinforcement and improvement. However, there are still certain restrictions on how this study may be used to practical engineering, such as the impact of microbial strains' working settings, the uniformity of the spraying technique, the impact of harsh environments, etc.

Acknowledgements This work was supported by the National Natural Science Foundation of China (51580166). Any opinions, findings, and conclusions or recommendations expressed in this material are those of the authors and do not necessarily reflect the views of the National Science Foundation. Thanks to Henan Polytechnic University for providing laboratory equipment and space, Thank you to all the participants and helpers of this work.

Author contributions The authors of ZM and FC did relevant experiments and wrote the main manuscript text, NS, XP and CC learned and applied relevant software technologies. All authors commented on previous versions of the manuscript. All authors read and approved the final manuscript.

Funding This work was supported by the National Natural Science Foundation of China (51580166).

Data availability The data are transparent.

Declarations

Conflict of interest The authors have no relevant financial or non-financial interests to disclose.

References

Al-Kharusi AS, Blunt MJ (2007) Network extraction from sandstone and carbonate pore space images. J Petrol Sci Eng 56(4):219–231

Bird MB, Butler SL, Hawkes CD, Kotzer T (2014) Numerical modeling of fluid and electrical currents through geometries based on synchrotron X-ray tomographic images of reservoir rocks using Avizo and COMSOL. Comput Geosci UK 73:6–16

Brian B, Robert PE (1998) Percolation theory and network modeling applications in soil physics. Surv Geophys 19(1):23–72

Cheng L, Cord-Ruwisch R (2014) Upscaling effects of soil improvement by microbially induced calcite precipitation by surface percolation. Geomicrobiol J 31(5):396–406

Cheng L, Cord-Ruwisch R, Shahin MA (2013) Cementation of sand soil by microbially induced calcite precipitation at various degrees of saturation. Can Geotech J 50(1):81–90

Cuthbert MO, McMillan LA, Handley-Sidhu S, Riley MS, Tobler DJ, Phoenix VR (2013) A field and modeling study of fractured rock permeability reduction using microbially induced calcite precipitation. Environ Sci Technol 47(23):13637–13643

DeJong JT, Fritzges MB, Nuesselein K (2006) Microbially induced cementation to control sand response to undrained shear. J Geotech Geoenviron 132(11):1381–1392

DeJong JT, Mortensen BM, Martinez BC, Nelson DC (2010) Biomediated soil improvement. Ecol Eng 36(2):197–210

Dejong JT, Soga K, Kavazanjian E, Burns S, Van Paassen LA, Al Qabany A, Aydilek A, Bang SS, Burbank M, Caslake LF, Chen CY, Cheng X, Chu J, Ciurli S, Esnault-Filet A, Fauriel S, Hamdan N, Hata T, Inagaki Y, Jefferis S, Kuo M, Laloui L, Larrahondo J, Manning DAC, Martinez B, Montoiz BM, Nelson DC, Palomion A, Renforth P, Santamarina JC, Seagren EA, Tanyu B, Tsesarsky M, Weaver T (2013) Biogeochemical processes and geotechnical applications: progress, opportunities and challenges. Géotechnique 63(4):287–301

Dimitrios T, Lyesse L (2019) A decade of progress and turning points in the understanding of bio-improved soils: a review. Geomech Energy Environ 19:100116

Dong H, Blunt MJ (2009) Pore-network extraction from micro-computerized-tomography images. Phys Rev E Stat Nonlin Soft Matter Phys 80(3 Pt 2):36307

Fan N, Wang J, Deng C, Fan Y, Wang T, Guo X (2020) Quantitative characterization of coal microstructure and visualization seepage of macropores using CT-based 3D reconstruction. J Nat Gas Sci Eng 81:103384

Fatt I (1956) The network model of porous media. Trans AIME 207(01):144–181

Fujita Y, Taylor JL, Wendt LM, Reed DW, Smith RW (2010) Evaluating the potential of native ureolytic microbes to remediate a 90Sr contaminated environment. Environ Sci Technol 44(19):7652–7658

Gomez MG, Anderson CM, Graddy CM, DeJong JT, Nelson DC, Ginn TR (2016) Large-scale comparison of bioaugmentation and biostimulation approaches for biocementation of sands. J Geotechn Geoenviron Eng. https://doi.org/10.1061/(ASCE)GT.1943-5606.0001640

Ivanov V, Chu J (2008) Applications of microorganisms to geotechnical engineering for bioclogging and biocementation of soil in situ. Rev Environ Sci Biotechnol 7(2):139–153

Ivanov AL, Shein EV, Skvortsova EB (2019) Tomography of soil pores: from morphological characteristics to structural-functional assessment of pore space. Eurasian Soil Sci 52(1):50–57

Koestel J, Larsbo M, Jarvis N (2020) Scale and REV analyses for porosity and pore connectivity measures in undisturbed soil. Geoderma 366:114206

Li TC, Shao MA, Jia YH (2016) Application of X-ray tomography to quantify macropore characteristics of loess soil under two perennial plants. Eur J Soil Sci 67(3):266–275

Li X, Lu Y, Zhang X, Fan W, Lu Y, Pan W (2019) Quantification of macropores of Malan loess and the hydraulic significance on slope stability by X-ray computed tomography. Environ Earth Sci 78(16):1–19

Liu L, Shen Y, Liu HL, Chu J (2016) Application of bio-cement in erosion control of leveas. Rock Soil Mech 37(12):3410–3416

Meng H, Gao Y, He J, Qi Y, Hang L (2021a) Microbially induced carbonate precipitation for wind erosion control of desert soil: field-scale tests. Geoderma 383:114723

Meng JQ, Zhang S, Cao ZH, Wang C (2022) Insight on coal molecular-scale pore reconstruction of Tunliu mine and its characterization and analysis. J China Coal Soc 47(s1):160–170

Meyer FD, Bang S, Min S, Stetler LD, Bang SS (2011) Microbiologically-induced soil stabilization: application of *Sporosarcina pasteurii* for fugitive dust control. In: Geo-frontiers 2011: advances in geotechnical engineering, pp 4002–4011

Mitchell JK, Santamarina JC (2005) Biological considerations in geotechnical engineering. J Geotechn Geoenviron Eng 131(10):1222–1233

Montoya BM, Dejong JT, Boulanger RW (2013) Dynamic response of liquefiable sand improved by microbial-induced calcite precipitation. Géotechnique 63(4):302–312

Naeimi M, Chu J (2017) Comparison of conventional and biotreated methods as dust suppressants. Environ Sci Pollut Res 24(29):23341–23350

Phillips AJ, Gerlach R, Lauchnor E, Mitchell AC, Cunningham AB, Spangler L (2013) Engineered applications of ureolytic biomineralization: a review. Biofouling (chur, Switzerland) 29(6):715–733

Phillips AJ, Cunningham AB, Gerlach R, Hiebert R, Hwang C, Lomans BP, Westrich J, Mantilla C, Kirksey J, Esposito R, Spangler L (2016) Fracture sealing with microbially-induced calcium carbonate precipitation: a field study. Environ Sci Technol 50(7):4111–4117

Sharma M, Satyam N, Reddy KR (2021) Effect of freeze-thaw cycles on engineering properties of biocemented sand under different treatment conditions. Eng Geol 284:106022

Silin D, Patzek T (2006) Pore space morphology analysis using maximal inscribed spheres. Physica A 371(2):336–360

Tang CS, Yin LY, Jiang NJ, Zhu C, Zeng H, Li H, Shi B (2020) Factors affecting the performance of microbial-induced carbonate precipitation (MICP) treated soil: a review. Environ Earth Sci 79(5):1–23

Terzis D, Laloui L (2018) 3-D micro-architecture and mechanical response of soil cemented via microbial-induced calcite precipitation. Sci Rep. https://doi.org/10.1038/s41598-018-19895-w

Terzis D, Laloui L (2019) Cell-free soil bio-cementation with strength, dilatancy and fabric characterization. Acta Geotech 14(3):639–656

van Paassen LA, Ghose R, van der Linden TJ, van der Star WR, van Loosdrecht MC (2010) Quantifying biomediated ground improvement by ureolysis: large-scale biogrout experiment. J Geotechn Geoenviron Eng 136(12):1721–1728

Whiffin VS (2004) Microbial $CaCO_3$ precipitation for the production of biocement. Murdoch University, Perth

Whiffin VS, van Paassen LA, Harkes MP (2007) Microbial carbonate precipitation as a soil improvement technique. Geomicrobiol J 24(5):417–423

Wu Y, Tahmasebi P, Lin C, Zahid MA, Dong C, Golab AN, Ren L (2019) A comprehensive study on geometric, topological and fractal characterizations of pore systems in low-permeability reservoirs based on SEM, MICP, NMR, and X-ray CT experiments. Mar Petrol Geol 103:12–28

Xie ZY, Zhang W, Yao TF, Wang J, Zhu YC (2020) Quantitative characte rization of spatial pore network of soils based on maximal-balls algorithm. J Eng Geol 28(01):60–68

Xu YB, Qian CX, Lu ZW (2013) Remediation of heavy metal contaminated soils by bacteria biomineralization. Chin J Environ Eng 7(07):2763–2768

Zhan Q, Qian C, Yi H (2016) Microbial-induced mineralization and cementation of fugitive dust and engineering application. Constr Build Mater 121:437–444

Zhang M, Wang R, Liu F, Xu P (2021) Anti-wind erosion and anti-dust mechanisms of microbial consolidation of bare soil. Environ Earth Sci 80(21):1–13